

Role of viscosity in fusion-fission dynamics via simultaneously measured neutron and α -particle multiplicities

K. Kapoor, N. Bansal, Chetan Sharma, S. Verma, K. Rani, R. Mahajan, B. R. Behera, K. P. Singh, and A. Kumar*

Department of Physics, Panjab University, Chandigarh 160014, India

H. Singh

Department of Physics, Kurukshetra University, Kurukshetra 136119, India

R. Dubey, N. Saneesh, M. Kumar, A. Yadav, A. Jhingan, and P. Sugathan

Inter University Accelerator Centre, New Delhi 110067, India

B. K. Nayak and A. Saxena

Nuclear Physics Division, Bhabha Atomic Research Centre, Mumbai 400085, India

H. P. Sharma

Department of Physics, Banaras Hindu University, Varanasi 221005, India

S. K. Chamoli

Department of Physics and Astrophysics, University of Delhi, Delhi 110007, India



(Received 21 November 2018; revised manuscript received 5 March 2019; published 31 July 2019)

The multiplicities of α particles and neutrons have been measured simultaneously for the reaction $^{16}\text{O} + ^{196}\text{Pt}$ forming ^{212}Rn compound nucleus at excitation energies of 56 MeV, 61 MeV, and 68 MeV. Neutrons and α particles were detected at various angles in coincidence with the fission fragments. To extract the contribution of pre- and postmultiplicities using the total α -particle and neutron spectra, moving source formalism was implemented. In the case of α particle, near scission contribution has also been extracted. Study of the fission mechanism using light particle emissions are helpful in understanding the detailed fusion-fission reaction dynamics. The statistical model code JOANNE2, which includes deformation-dependent particle transmission coefficients, binding energies and level densities, has been used to reproduce the measured multiplicities of neutrons and α particles by varying the transient (τ_{tr}) and saddle to scission (τ_{ssc}) times. It is found that the fission time scales of the order of $50\text{--}70 \times 10^{-21}$ sec are required to reproduce the neutron and α -particles multiplicities simultaneously. The fission time scales are the measure of the nuclear viscosity, which is responsible for the dynamic hindrance of the fission process.

DOI: [10.1103/PhysRevC.100.014620](https://doi.org/10.1103/PhysRevC.100.014620)

I. INTRODUCTION

Study of the reaction dynamics involved in the heavy-ion-induced nuclear reactions has been one of the important area of interest in nuclear physics research. The compound nucleus formed in heavy-ion reaction has the probability to proceed towards the fission process depending on the available excitation energy, temperature. Fusion-fission dynamics of the excited nucleus can be studied by characterizing the emitted particles, such as α , p , ν , and γ during the course of deexcitation [1,2]. As compared to that given by the transition-state theory of Bohr and Wheeler [3], there is a clear excess of the measured pre-scission multiplicities of neutrons [4,5], charged particles [2,6,7], and giant dipole resonance (GDR)

[8]. The excess indicates a hindrance or slowing down of the fission process. In statistical code, the slowing down of fission process is usually taken into account by using Kramers' expression for the fission width, which considers a dissipative dynamics for fission [9] resulting in the longer fission time. From comparison of the multiplicity data with theoretical model calculation one can derive the pre-scission time scale and friction coefficient. It has been observed that the fission process slows down to an order (10^{-20} – 10^{-19} s) due to nuclear viscosity [10]. During the fission process, emission of the particles is divided into two major components: particles emitted from the compound nucleus called pre-scission particles whereas the particles emitted from the fragments called postscission particles [6]. Fission time is divided into two major parts: time needed for transition from equilibrium compound state to saddle point called the transient time (τ_{tr}) and the time of descent from saddle to scission point called

*Corresponding author: ashok@pu.ac.in

τ_{ssc} . Investigation of the emitted particles provides information about the dynamical and statistical aspects of the fission process [7]. During the separation of two nuclei at the scission point, large kinematic focusing plays an important role in the fission dynamics [11]. The charged particle emission taking place near the neck region just before the scission is termed as near-scission emission (NSE).

The main bulk of the information about the fusion-fission dynamics of heated rotating nuclei formed in heavy-ion-induced reactions have been obtained with neutron measurements and indicate that the fission process is dissipative in nature at high excitation energy. There are some measurements also where charged particles are used as a probe to study the fusion-fission dynamics. But there are very few measurements where the charged particles and neutron multiplicities have been measured simultaneously. To understand the dynamics involved in the fission, in the present work, we have measured simultaneously the α -particle and neutron multiplicities for compound nucleus ^{212}Rn at various excitation energies. Standard statistical model code JOANNE2 [12,13] has been used to reproduce the measured α -particle and neutron multiplicity by varying the fission time scales. The experimental setup used in the present work has been discussed in Sec. II. Section III describes the details about the procedure to extract the τ_{pre} , and τ_{post} and NSE contributions. For α_{NSE} contribution has also been extracted. Section IV describes the details of the standard statistical model analysis to reproduce the experimentally measured multiplicities using JOANNE2 code followed by summary and acknowledgments.

II. EXPERIMENTAL DETAILS

The experiment was performed with 15UD Pelletron facility at Inter University Accelerator Centre (IUAC), New Delhi, using General Purpose Scattering Chamber (GPSC). A self-supporting enriched target of ^{196}Pt having a thickness of 1.8 mg/cm^2 was used in the experiment. A pulsed beam of ^{16}O at energy 93, 99, and 106 MeV was bombarded on ^{196}Pt to form ^{212}Rn compound nucleus at the excitation energy of 56 MeV, 61 MeV, and 68 MeV. Multi Wire Proportional Counter (MWPC) detectors were used for the detection of fission fragments. MWPC detector was made up of four electrodes: anode, cathode, and position signals [14]. Two MWPC detectors were kept at the folding angles so as to detect complementary fission fragments. One of the MWPC detectors was kept at an angle of 30° with respect to beam direction whereas the second MWPC detector was kept at an angle of 135° with respect to beam and were at the distance of 20.5 cm from the center of the target. These MWPC detectors were having an active area of $(20 \text{ cm} \times 10 \text{ cm})$. The fast timing signal from the MWPCs were used to get the time-of-flight (TOF) information of the fission fragments with reference to the beam arrival time, which enabled us to separate the fission events from other competing channels. Two passivated implanted planar silicon (PIPS) detectors were also placed inside the scattering chamber at $\pm 10^\circ$ as monitors.

The detector system used in the current setup has 16 CsI(Tl) crystals, each having an area of $20 \text{ mm} \times 20 \text{ mm}$ with thickness of 3 mm. CsI(Tl) detector were kept at a

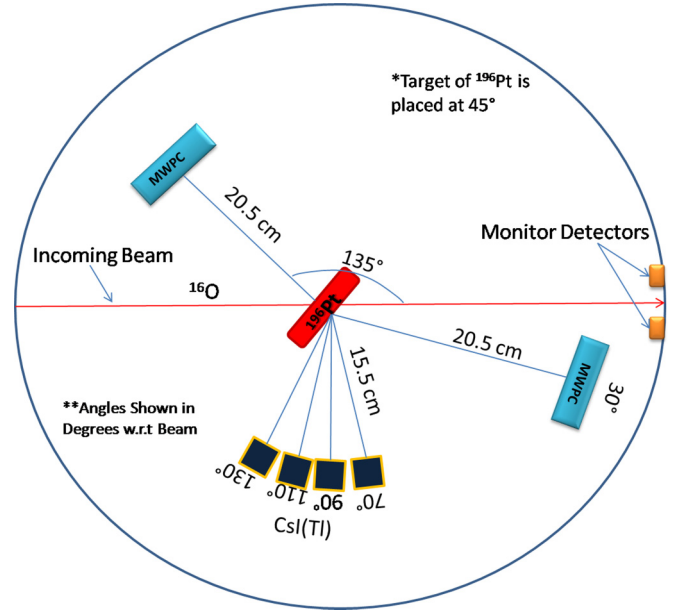


FIG. 1. Schematic diagram of experimental setup representing fission detectors as MWPC 1 and 2 kept at folding angle and charged particle detectors CsI(Tl) kept at 70° , 90° , 110° , and 130° with respect to MWPC detector at 30° .

distance of 15.5 cm from the center of the target. The schematic diagram of the experimental setup is shown in Fig. 1. The neutron detectors are not shown in the figure.

In order to differentiate between different particles, ballistic deficit pulse shaping technique was used to obtain two decay times, long decay time (τ_L) and short decay time (τ_S). Plotting long decay time to short decay time gives bands corresponding to different particles as shown in Fig. 2. The details of the procedure are given in our previous publications [15].

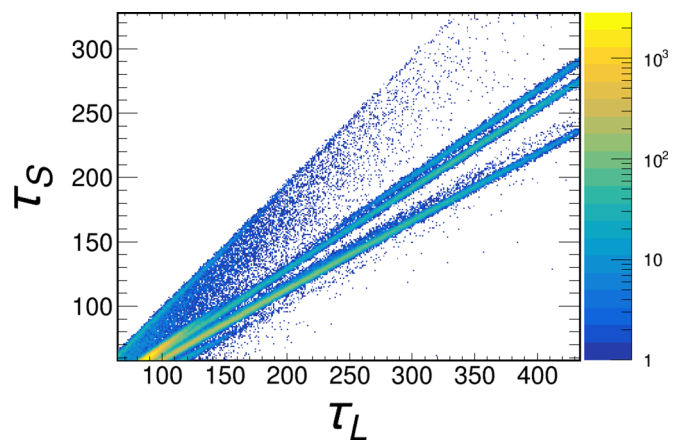


FIG. 2. Two-dimensional plot of long shaping time (τ_L) vs short shaping time (τ_S), representing different bands corresponding to different particles. γ from photodiode are seen in the top band. Second and third band represents protons and deuterons, respectively, whereas the bottom band represents α particles.

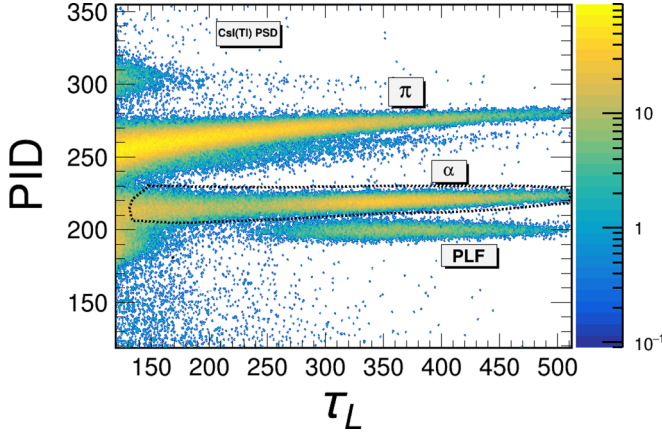


FIG. 3. Particle identification plot with PID on Y axis and long shaping time (τ_L) on X axis. Black marked band represents the α -particles band

The particle identification (PID) plot was obtained by taking the difference between τ_L and τ_S divided by τ_L .

$$\text{PID} = \frac{\tau_L - \tau_S}{\tau_L}. \quad (1)$$

Two-dimensional view of the obtained spectra is shown in Fig. 3.

Energy calibration of CsI(Tl) detectors for α particles was performed using ^{254}Am and ^{229}Th sources giving α energies up to 8 MeV. The in-beam calibration of the CsI(Tl) detectors was also performed using $^{12}\text{C}(^{12}\text{C}, \alpha)^{20}\text{Ne}^*$ and $^7\text{Li}(^{12}\text{C}, \alpha)^{15}\text{N}^*$ reactions at 30 MeV and 20 MeV, respectively, which provide discrete α energies ranging from 5 MeV–25 MeV corresponding to ^{20}Ne , ^{15}N states. During the in-beam calibration, all the four CsI(Tl) detectors were brought near beam axis at $\pm 10^\circ$ and $\pm 20^\circ$ to minimize the kinematic broadening.

Three neutron detectors (BC501) were also placed at 1.5 m from the center of target at angles 30° , 90° , and 120° with respect to beam direction. In order to reduce the background, the beam dump was placed 3 m downstream from the target and the beam line was shielded with paraffin and lead bricks. The threshold of the neutron detectors was kept at about 0.5 MeV by calibrating it with the standard sources (^{137}Cs and ^{60}Co) [16]. The trigger of the data acquisition was generated by logical OR of the two fission fragments (cathode of the two MWPCs) and charged particle detectors, which was further AND-gated with the RF of the beam. Fission-gated neutron and α -particle spectra were obtained by normalizing with total fission after correcting for random coincidence.

III. DATA ANALYSIS

During the off-line data analysis, MWPC fission detector was divided into four equal parts in order to have the better angle definitions. Each slicing had a bin size of $\approx 7.5^\circ$ forming various angles with respect to beam as well as CsI(Tl) and neutron detector. Different values of relative angles i.e., angle of the α -particle detector with respect to beam (Θ_α), angle of the α -particle detector with respect to fission detector (MWPC 1) (Θ_α), and angle of the α -particle detector with

respect to another fission detector (MWPC 2) ($\Theta_{\alpha f2}$) were generated. Similarly, different angle combinations of neutron detectors with respect to beam and fission detectors have been obtained. Final α -particle and neutron multiplicity spectra were obtained at various angles by dividing the coincidence spectra with the total fission counts and the solid angle of the detector. In total, eight combinations for (Θ_α), ($\Theta_{\alpha f1}$), and ($\Theta_{\alpha f2}$) were obtained. The normalized α particles and neutrons spectra, thus obtained, were fitted simultaneously with moving source model considering three sources namely: compound nucleus, complementary fission fragments and the near scission emission (NSE). In case of α particles, fourth source, near scission emission (NSE), has also been considered. In the moving source analysis, fission is assumed to be symmetric and mean values of fragment mass and charge are used. The α -particles and neutrons emission is assumed to be isotropic in the rest frames of sources and energy spectra are calculated using the constant temperature level density expression [6] given below,

$$n(\epsilon) \approx \alpha_p \epsilon \sigma(\epsilon) \exp\left(\frac{-\epsilon}{T}\right), \quad (2)$$

where α_p and ϵ are the multiplicity and the energy of the emitted α particles in the rest frame, T is the temperature of the source and $\sigma(\epsilon)$ is the inverse reaction cross section. The inverse reaction cross section was calculated using Wong's formula [17].

$$\sigma(\epsilon) = \frac{\hbar\omega R^2}{2\epsilon} \log \left\{ 1 + \exp \left[\frac{2\pi}{\omega} (\epsilon - V_B) \right] \right\}, \quad (3)$$

where $\hbar\omega$ is the curvature of fusion barrier for angular momentum (ℓ) = 0. The pre- and postscission values for $\hbar\omega$ used in moving source analysis were 4.8 and 4.0 MeV, respectively [6]. Temperature (T) for the pre- and postscission sources was calculated using formula:

$$T = \sqrt{\frac{E^*}{a}}, \quad (4)$$

where E^* is the intrinsic excitation energy of the source and a represents the level density parameter, which was taken as $A/11$ for the compound nucleus and $A/7$ for the fission fragments [6]. The values for T_{pre} and T_{post} were calculated to be 1.52 and 1.1 MeV, respectively, after scaling down T_{pre} by a factor of 11/12 to account for the multistep evaporation [18]. The Coulomb barrier for α particles (V_B) at the exit channel was calculated using the following expression [19]:

$$V_B = \frac{1.44Z_P(Z_S - Z_P)}{r_0[(A_P)^{(1/3)} + (A_S - A_P)^{(1/3)}] + \delta} \text{ MeV}, \quad (5)$$

where A_P , Z_P , and A_S , Z_S are the masses and charges of the α -particle and emitting sources, respectively. The value of r_0 was taken as 1.45 fm. The parameter δ was used to take care for the reduction in barrier due to the deformation effects of the sources and was taken as 2.0 for compound nucleus and 0.4 for the fission fragments. The values of $V_{\text{pre}}^B = 20.8$ MeV, and $V_{\text{post}}^B = 12.7$ MeV were used in moving source code for pre- and postscission sources, respectively. The study of NSE of α particles is important for understanding the collective

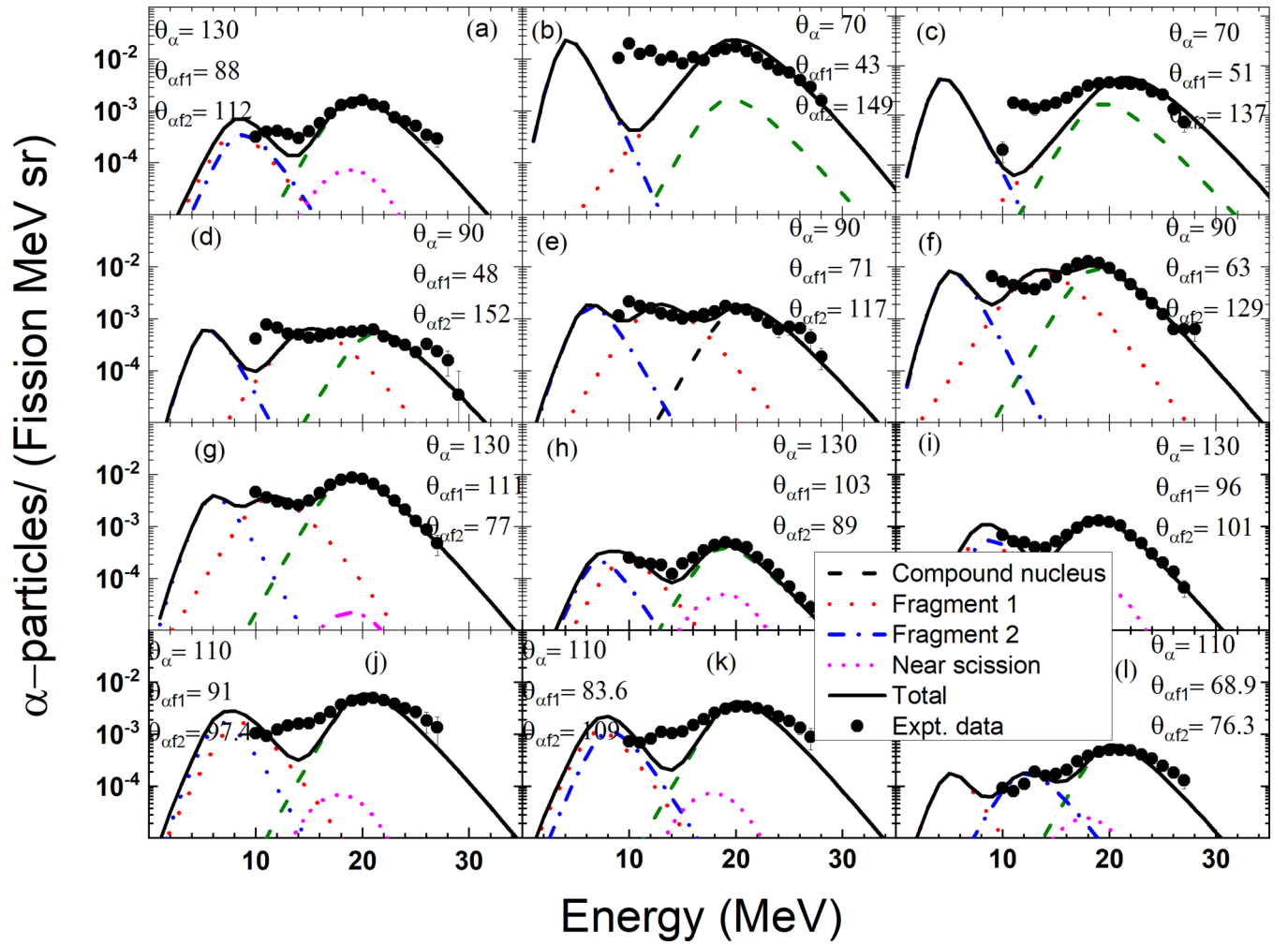


FIG. 4. Normalized α -particle multiplicity spectra at $E_{\text{lab}} = 93$ MeV, along with fits of moving source formula. These spectra are shown at various relative angles between the CsI(Tl) detectors and the fission detectors in laboratory frame. Various contributions are represented in different colors. Red and blue line represents the contribution from two fragments of postscission segments whereas the black line is representing the compound nucleus contributions or pre-scission segment and the neck contribution is represented by pink line or near scission emission. Total contribution is shown in green color. The error bars represent the statistical errors only.

fission dynamics and can provide valuable information on the scission point characteristics. This emission is assumed to take place at scission point almost similar to the ternary fission at low energy. It is well established in low-energy fission that NSE has an energy distribution which is nearly Gaussian and an angular distribution, which has a noticeable dependence on the energy of the emitted particles [7]. Since the mechanism of NSE α particles in heavy-ion reactions is still not clear, so for simplicity we have assumed that both the energy and the angular distribution have Gaussian forms and are independent of each other. Therefore, in order to extract the NSE contribution to α -particle spectra in the moving source analysis, the energy and angular distribution were assumed to be Gaussian in the rest frame and the following expression was used [2]:

$$\eta(\epsilon, \theta) \approx \alpha_{\text{NSE}} \exp\left[-\frac{(\epsilon - \epsilon_p)^2}{2\sigma_\epsilon^2}\right] \exp\left[-\frac{(90 - \theta)^2}{2\sigma_\theta^2}\right], \quad (6)$$

where α_{NSE} is the α -particle multiplicity of the NSE, ϵ_p is the peak or mean energy of α particle, θ is the relative angle of α particle with respect to scission axis, σ_ϵ is standard deviations of the energy distribution and σ_θ is the width of angular distribution in the rest frame. Near scission emission is assumed to be dominating in perpendicular direction to scission axis.

The α -particle spectra from four sources were calculated in rest frame using Eqs. (3), (4), and (7) and then were converted to laboratory frames using the appropriate Jacobians. The spectra thus obtained from the individual four sources were summed up to have total α spectra. The mean fragment velocities were determined using Viola's systematic [20] for the total kinetic energy released in fission process. The temperatures (T_{pre} , T_{post}) and Coulomb barriers (V_{pre}^B and V_{post}^B) were fixed during the moving source analysis to extract the pre-scission, postscission, and NSE contributions. The pre-scission, postscission, and NSE multiplicities were kept

TABLE I. Experimentally measured α particle, neutron multiplicities, and temperatures for $^{16}\text{O} + ^{196}\text{Pt}$ reaction.

S. No	E^* (MeV)	α_{pre}	α_{post}	ν_{pre}	ν_{post}	T_{pre} (MeV)	T_{post} (MeV)	τ_{ssc} (zs)
1	56	$(7.20 \pm 0.13) \times 10^{-3}$	$(0.49 \pm 0.013) \times 10^{-3}$	(2.30 ± 0.07)	(0.78 ± 0.03)	1.46	1.31	50
2	61	$(1.02 \pm 0.5) \times 10^{-2}$	$(0.17 \pm 0.02) \times 10^{-2}$	(2.53 ± 0.05)	(0.91 ± 0.02)	1.52	1.34	62
3	68	$(1.86 \pm 0.24) \times 10^{-2}$	$(0.63 \pm 0.05) \times 10^{-2}$	(2.98 ± 0.09)	(0.88 ± 0.05)	1.58	1.39	70

as free parameters during the fitting. Figure 4 shows fitted spectra for the individual sources along with total spectra at various angles at incident energy of 93 MeV. Various contributions are marked with different color schemes. Values of the multiplicities obtained from the best fit are given in Table I. In these values of multiplicity, systematic errors have not been included. One of the main sources of systematic errors in the multiplicity may be the temperature.

In the present work, we have used the level density parameter $a = A/11$ taken from the work of Gupta *et al.* [6]. In the literature, however, this parameter has also been taken as $A/10$. We found that if level density parameter is taken $A/10$, then the multiplicity increases by ≈ 10 times. Moreover it can be seen in Fig. 4, that the neck emission is more dominant where the angle between fission fragment and the emitted charged particle is approaching towards 90° , whereas it decreases at smaller angles. This is due to the Coulomb focusing in the perpendicular direction. In case of neutrons, the time-of-flight spectra was converted into energy spectra. Since

neutron detector (BC501) is sensitive to both γ and neutrons so particle identification between the two were done using pulse shape discrimination method based on zero-crossover technique [21]. The TOF of neutrons were converted into neutron energy by considering the prompt γ peak in the TOF spectrum for reference time. The energy of the neutron was obtained using the formula:

$$E_n = \frac{mL^2}{2t^2}, \quad (7)$$

where L is the flight path or distance of the detector from the center of the target, m is the mass of neutron, and t is the TOF. The Jacobians were appropriately introduced to convert the TOF spectra into the energy spectra. The obtained neutron energy distribution was corrected for the energy-dependent efficiency of each detector. The efficiency curve of the neutron detector as a function of neutron energy was obtained by using the Monte Carlo computer code MODEFF [19]. Neutron energy spectrum was normalized to the fission events. Normalized

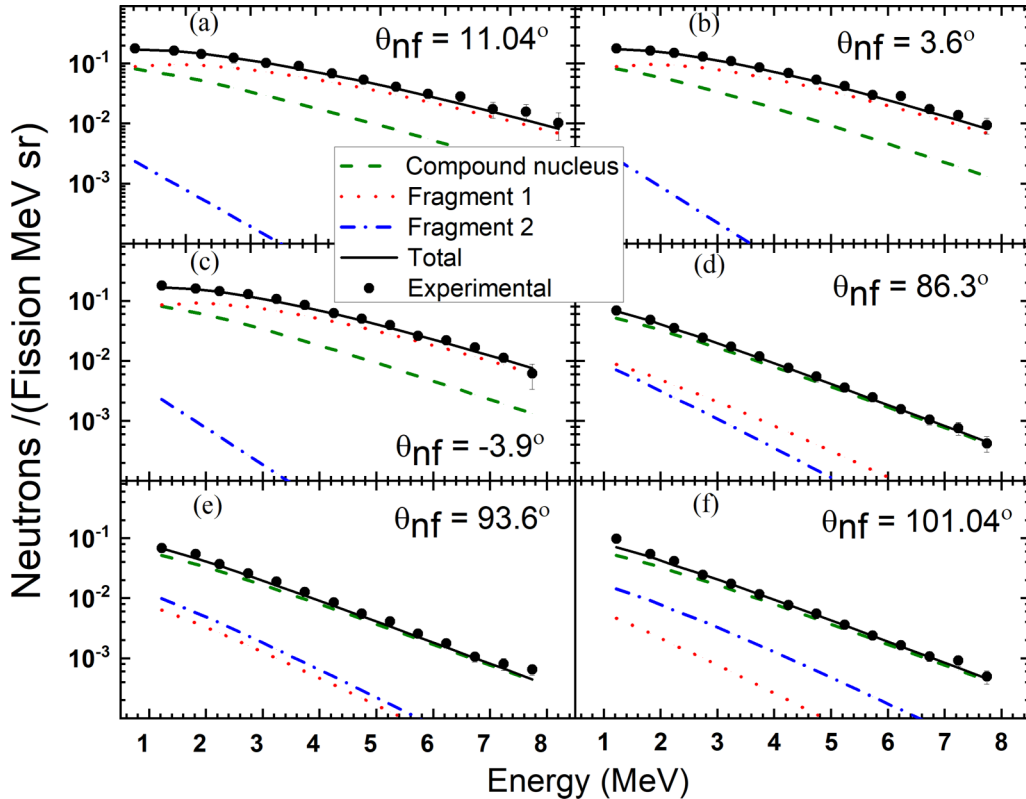


FIG. 5. Normalized neutron multiplicity spectra at $E_{\text{lab}} = 93$ MeV, along with fits with moving source formula. These spectra are shown at various relative angles between the neutron detectors and the fission detectors in laboratory frame. Various contributions are represented in different colors. Red and blue line represents the contribution from two fragments or postscission segments whereas the black line is representing the compound nucleus contributions or pre-scission segment. Total contribution is shown in pink color.

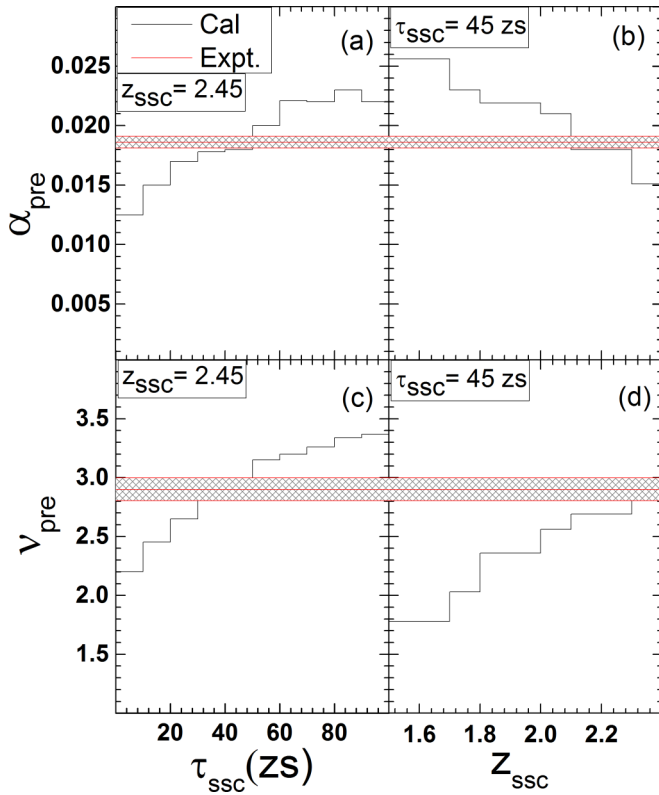


FIG. 6. The variation of ν_{pre} and α_{pre} as a function τ_{ssc} in (a) and (c) and as a function of Z_{ssc} in (b) and (d) for $^{16}\text{O} + ^{196}\text{Pt}$. The shaded region corresponds to value of ν_{pre} and α_{pre} .

neutron yield spectra were fitted at various angles using the moving source technique to extract the multiplicities.

Neutron multiplicities were calculated for three sources namely: compound nucleus and the two fragments sources. The pre- and postscission contributions were derived from various angles combinations using the Watt expression [22,23]. The neutrons emitted from compound nucleus are known as pre-scission whereas the neutrons emitted from the fully accelerated fission fragments are known as postscission. Neutron emissions from different sources are assumed to be isotropic in their rest frames. Neutron multiplicities are derived using the formula:

$$\frac{d^2 M_n}{dE_n dW_n} = \sum_{i=1}^3 \frac{M_{n_i} \sqrt{E_n}}{2(\pi T_i)^{3/2}} \exp \left\{ \frac{E_n - 2\sqrt{\frac{E_n E_i}{A_i}} \cos \theta_i + \frac{E_i}{A_i}}{T_i} \right\}, \quad (8)$$

where E_n is the energy of the neutron in laboratory frame, E_i is the energy, T_i is the temperature, and M_{n_i} is the multiplicity of the neutrons. A_i is the mass of source of neutron where θ_i is the relative angle between the respective source direction and the emitted neutrons. Fission fragments kinetic energy calculations were carried out using the Viola's kinematic for the symmetric fission. The pre- and postscission neutron multiplicities and temperatures denoted by M_{pre} , M_{post} , T_{pre} , and T_{post} respectively, were determined from the least-square fits considering them as free parameters. The postscission emission parameters M_{post} and T_{post} are considered to be

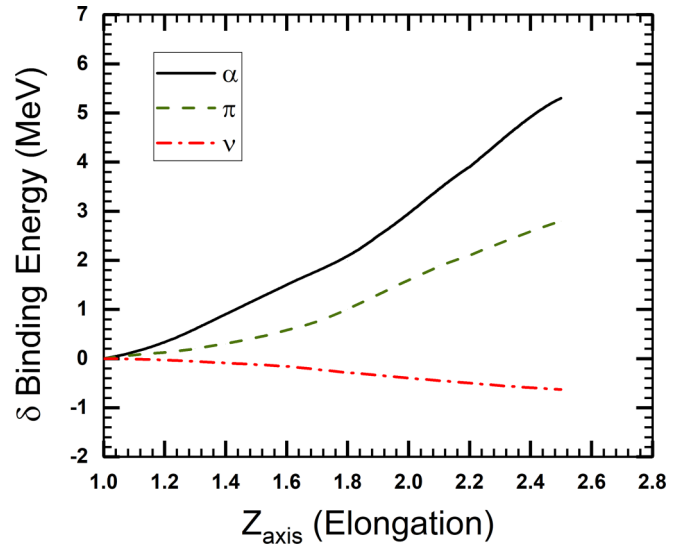


FIG. 7. Deformed liquid drop model predictions of the deviation of binding energies from spherical nucleus for neutron, proton, and α -particle emission.

same for both the fission-fragments. The temperatures were considered in the same way as in case of α . Normalized neutron spectra at incident energy of 93 MeV along with fits using moving source formalism are shown in Fig. 5.

IV. STATISTICAL MODEL CALCULATIONS

JOANNE2 [13] code, which incorporates the deformation-dependent particle binding energies and transmission coefficients, was used to reproduce the simultaneously measured neutron and α particle pre-scission multiplicities. In this model, it is assumed that the pre-scission particle emission takes place from two points in deformation space. First corresponds to mean presaddle deformation (Z_{tr}) and second to mean saddle to scission deformation (Z_{ssc}) where Z represents the elongation of the symmetry axis (in units of the diameter of the spherical nucleus). In mean presaddle time (τ_{tr}), particle emission takes place only from nearly spherical systems and then the fission decay competes with particle emission for mean saddle to scission time (τ_{ssc}). The relation between fission times (τ_{tr} , τ_{ssc}) and the nuclear viscosity has been explained by Lestone *et al.* [12]. The fission times provide the information about the strength of the viscosity of the nuclear medium. Larger values of the fission times scales represent the stronger nuclear viscosity. Level density parameters a_n for spherical compound nucleus and a_{ssc} at each Z_{ssc} for the saddle to scission, are calculated using the Toke and Swiatecki [10] formalism. Statistical calculations have been performed by varying presaddle time (τ_{tr}), saddle to scission time (τ_{ssc}), and deformation (Z_{ssc}) to observe their effect on ν_{pre} and α_{pre} . In our earlier work [24], we observed that if we take the value of Z_{ssc} near to the scission point, the ν_{pre} and α_{pre} values can be reproduced simultaneously for some values of τ_{ssc} and τ_{tr} .

Calculations for ν_{pre} and α_{pre} as a function of Z_{ssc} and (τ_{ssc}) for fixed Z_{tr} at 1.31 and $\tau_{tr} = 20$ zs are shown in Fig. 6. It can be seen in Figs. 6(a) and 6(c) that the value of ν_{pre} and α_{pre} ,

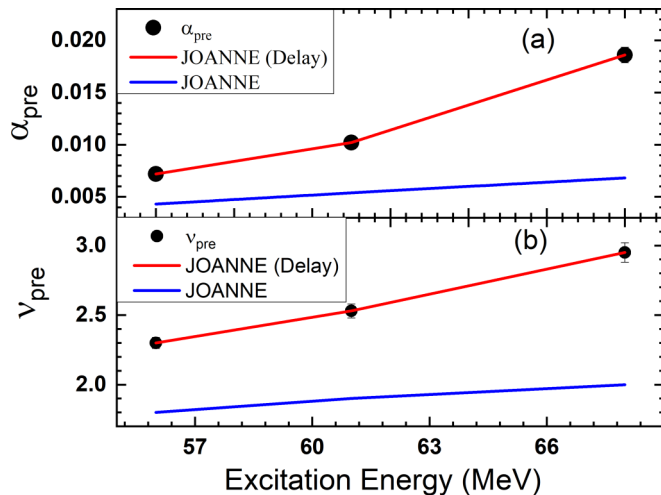


FIG. 8. Plot of ν_{pre} and α_{pre} as a function of excitation energy and JOANNE2 calculations with and without fission delay for $^{16}\text{O} + ^{196}\text{Pt}$.

with fixed Z_{ssc} , increases with increasing τ_{ssc} and to reproduce the experimentally obtained multiplicity for neutron and α , value of τ_{ssc} between 30–50 zs is required. Figures 6(b) and 6(d) represent the pre-scission α and neutron multiplicity, respectively, as a function of deformation in saddle to scission region. The experimentally obtained value is shown as red band. Figure 7 shows the variation of binding energies with deformation for neutron, proton, and α particles. It is clearly evident that pre-scission neutron multiplicity is seen to be increasing with the more elongation due to decrease in the neutron binding energy whereas pre-scission α multiplicity is seen to decrease with increasing binding energy. A clear overlap between the experimental and calculated values of the ν_{pre} and α_{pre} is seen for $\tau_{\text{ssc}} = 45$ zs in the near scission region. Analysis has been done with and without incorporating the delays in JOANNE2 code. As can be seen from Fig. 8, fission delays are required to reproduce experimentally obtained ν_{pre} and α_{pre} multiplicities, which increase with the excitation energy. As can be seen from Table I, fission delays increase with the excitation energy. In JOANNE2, the inserted delays are mimicking the role of viscosity and therefore, the

strength of the viscosity increase with excitation energy as larger delays are required at higher excitation energy to reproduce the measured particle multiplicities. In earlier neutron multiplicity measurements also [5,25,26], it was observed that pre-scission neutron multiplicities are underpredicted by the standard statistical model and that the fission dynamics of an excited compound nucleus is dissipative in nature at high excitation energies. The same observations have also been made from light charged particle multiplicities [6,13], GDR γ rays [27–29] and evaporation residue cross-section measurements [30,31].

V. SUMMARY AND CONCLUSION

In the present work, we have measured the α and neutron multiplicities simultaneously using $^{16}\text{O} + ^{196}\text{Pt}$ reaction at 93, 99, and 106 MeV forming ^{212}Rn nucleus. In the past, very few experiments have been performed where the charged particle and neutron multiplicity has been measured simultaneously. α and neutron's spectra were measured in coincidence with the fission fragments. Fitting of the particles spectra was performed with moving source code in order to extract the pre-scission and post-scission multiplicities for α and neutron. Near scission multiplicities for α particles have also been measured. Results were compared with statistical model code JOANNE2 to obtain α -particles and neutron pre-scission multiplicity. We found that both the neutron and α -particle multiplicity can be reproduced simultaneously if we introduce a fission delay $\tau_{\text{total}} = (50\text{--}70)$ zs, which represent the viscous nature of the nuclear medium.

ACKNOWLEDGMENTS

Authors would like to thank Pelletron accelerator staff of Inter University Accelerator Centre (IUAC), New Delhi for providing beam of excellent quality during the whole experiment. Authors are also thankful to Dr. Varinderjit Singh for providing the ^{196}Pt target. One of the authors, K.K., is also thankful of IUAC, New Delhi for providing financial assistance.

- [1] D. J. Hinde, R. J. Charity, G. S. Foote, J. R. Leigh, J. O. Newton, and A. S. Ogaza, *Nucl. Phys. A* **452**, 550 (1986).
- [2] K. Ramachandran, A. Chatterjee, A. Navin, K. Mahata, A. Shrivastava, V. Tripathi, S. Kailas, V. Nanal, R. G. Pillay, A. Saxena *et al.*, *Phys. Rev. C* **73**, 064609 (2006).
- [3] N. Bohr and J. A. Wheeler, *Phys. Rev.* **56**, 426 (1939).
- [4] A. Chatterjee, A. Navin, S. Kailas, P. Singh, D. C. Biswas, A. Karnik, and S. S. Kapoor, *Phys. Rev. C* **52**, 3167 (1995).
- [5] R. Sandal, B. R. Behera, V. Singh, M. Kaur, A. Kumar, G. Singh, K. P. Singh, P. Sugathan, A. Jhingan, K. S. Golda *et al.*, *Phys. Rev. C* **87**, 014604 (2013).
- [6] Y. K. Gupta, D. C. Biswas, R. K. Choudhury, A. Saxena, B. K. Nayak, B. John, K. Ramachandran, R. G. Thomas, L. S. Danu, B. N. Joshi *et al.*, *Phys. Rev. C* **84**, 031603 (2011).
- [7] J. P. Lestone, J. R. Leigh, J. O. Newton, D. J. Hinde, J. X. Wei, J. X. Chen, S. Elfstrom, and M. Zielinska-Pfabe, *Nucl. Phys. A* **559**, 277 (1993).
- [8] N. P. Shaw, I. Diószegi, I. Mazumdar, A. Buda, C. R. Morton, J. Velkovska, J. R. Beene, D. W. Stracener, R. L. Varner, M. Thoennessen *et al.*, *Phys. Rev. C* **61**, 044612 (2000).
- [9] H. A. Kramers, *Physica* **7**, 284 (1940).
- [10] J. Toke and W. J. Swiatecki, *Nucl. Phys.* **29**, 462 (1962).
- [11] D. J. Hinde, H. Ogata, M. Tanaka, T. Shimoda, N. Takahashi, A. Shinohara, S. Wakamatsu, K. Katori, and H. Okamura, *Phys. Rev. C* **39**, 2268 (1989).
- [12] J. P. Lestone and S. G. McCalla, *Phys. Rev. C* **79**, 044611 (2009).
- [13] J. P. Lestone, *Phys. Rev. Lett.* **70**, 2245 (1993).

- [14] A. Jhingan, P. Sugathan, K. S. Golda, R. P. Singh, T. Varughese, H. Singh, B. R. Behera, and S. K. Mandal, *Rev. Sci. Instrum.* **80**, 123502 (2009).
- [15] A. Jhingan, P. Sugathan, G. Kaur, K. Kapoor, N. Saneesh, T. Banerjee, H. Singh, A. Kumar, B. R. Behera, and B. K. Nayak, *Nucl. Instr. Meth. A* **786**, 51 (2015).
- [16] T. G. Masterson, *Nucl. Instrum. Methods* **88**, 61 (1970).
- [17] C. Y. Wong, *Phys. Rev. Lett.* **31**, 766 (1973).
- [18] Y. K. Gupta, D. C. Biswas, B. John, B. K. Nayak, A. Chatterjee, and R. K. Choudhury, *Phys. Rev. C* **86**, 014615 (2012).
- [19] R. Yanez, T. A. Bredeweg, E. Cornell, B. Davin, K. Kwiatkowski, V. E. Viola, R. T. de Souza, R. Lemmon, and R. Popescu, *Phys. Rev. Lett.* **82**, 3585 (1999).
- [20] V. E. Viola, K. Kwiatkowski, and M. Walker, *Phys. Rev. C* **31**, 1550 (1985).
- [21] S. Venkataramanan, A. Gupta, K. S. Golda, H. Singh, R. Kumar, R. P. Singh, and R. K. Bhowmik, *Nucl. Instrum. Methods Phys. Res. A* **596**, 248 (2008).
- [22] A. Saxena, A. Chatterjee, R. K. Choudhury, S. S. Kapoor, and D. M. Nadkarni, *Phys. Rev. C* **49**, 932 (1994).
- [23] D. Hilscher, J. R. Birkelund, A. D. Hoover, W. U. Schroder, W. W. Wilcke, J. R. Huizenga, A. C. Mignerey, K. L. Wolf, H. F. Breuer, and V. E. Viola, *Phys. Rev. C* **20**, 576 (1979).
- [24] K. Kapoor, S. Verma, P. Sharma, R. Mahajan, N. Kaur, G. Kaur, B. R. Behera, K. P. Singh, A. Kumar, H. Singh *et al.*, *Phys. Rev. C* **96**, 054605 (2017).
- [25] D. Hilscher and H. Rossner, *Ann. Phys. Fr.* **17**, 471 (1992).
- [26] J. Cabrera, Th. Keutgen, Y. E. Masri, Ch. Dufauquez, V. Roberfroid, I. Tilquin, J. Vann Mol, R. Regimbart, R. J. Charity, J. B. Natowitz *et al.*, *Phys. Rev. C* **68**, 034613 (2003).
- [27] H. Rossner, D. Hilscher, D. J. Hinde, B. Gebauer, M. Lehmann, M. Wilpert, and E. Mordhorst, *Phys. Rev. C* **40**, 2629 (1989).
- [28] D. J. Hofman, B. B. Back, and P. Paul, *Phys. Rev. C* **51**, 2597 (1995).
- [29] H. Rossner, D. J. Hinde, J. R. Leigh, J. P. Lestone, J. O. Newton, J. X. Wei, and S. Elfstrom, *Phys. Rev. C* **45**, 719 (1992).
- [30] B. B. Back, D. J. Blumenthal, C. N. Davids, D. J. Henderson, R. Hermann, D. J. Hofman, C. L. Jiang, H. T. Penttila, and A. H. Wuosmaa, *Phys. Rev. C* **60**, 044602 (1999).
- [31] C. R. Morton, D. J. Hinde, J. R. Leigh, J. P. Lestone, M. Dasgupta, J. C. Mein, J. O. Newton, and H. Timmers, *Phys. Rev. C* **52**, 243 (1995).